RSC Advances

ROYAL SOCIETY OF CHEMISTRY

www.rsc.org/advances

Graphical abstract

Novel $ZnGa_2O_4$ nanorod arrays have been controlled synthesized from hexagonal ZnO microdishes; high photocatalytic activity was demonstrated for the degradation of Rh B under UV light radiation.

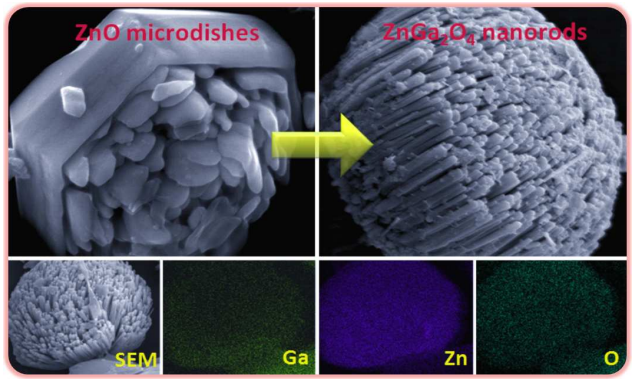

Journal Name

RSCPublishing

COMMUNICATION

Controlled synthesis of $ZnGa_2O_4$ nanorod arrays from hexagonal ZnO microdishes and their photocatalytic activities on degradation of RhB

11Cite this: DOI: 10.1039/x0xx00000x

Received 00th January 2012,
Accepted 00th January 2012

DOI: 10.1039/x0xx00000x

www.rsc.org/

Zesheng Li,*[a] Bolin Li,[a] Zhenghui Liu,[a] Dehao Li,[a] Chunyu Ge,[b] Yueping Fang*[b]

[a] *Development Center of Technology for Petrochemical Pollution Control and Cleaner Production of Guangdong Universitites, College of Chemical Engineering, Guangdong university of Petrochemical Technology, Maoming, Guangdong, 525000, China;*
[b] *Institute of Biomaterial, College of Science, South China Agricultural University, Guangzhou, 510642, China.*
Corresponence author: Zesheng Li E-mail: lzs212@163.com; Yueping Fang E-mail: ypfang@scau.edu.cn.

Novel $ZnGa_2O_4$ nanorod arrays with desirable photocatalytic activity for organic dye degradation have been synthesized, by an associated solution-liquid-solid growth and topological-morphology-conversion synthetic strategy.

Manipulating the physical dimensions and chemical compositions of semiconductors has attracted intensive attention due to their important roles in determining physicochemical properties of the materials.[1] The emergence and application of nanotechnology has provided great exciting advances in controlling the structure and morphology of semiconductors.[2] Among various nanostructures, one-dimensional (1-D) nanostructures, such as wires, tubes, rods and belts have attracted intense research interest because they exhibit lots of outstanding properties in optical, electronic, and catalytic fields.[3] Compared with conventional bulk materials and 0-D structures (e.g., nanoparticles), 1-D nanostructures can improve the transport of charge carriers and thus reduce the recombination losses at grain boundaries.[4] Particularly, the aligned 1-D nanostructures formed by the directed self-assembly of nanorods, nanowires and nanotubes, are a class of novel 1-D oriented architectures, which can give rise to extraordinary collective properties.[5] Such self-supported 1-D arrays are demonstrated to have high performances in catalysis systems for photocatalytic degradation of organic dye[6] and air purification[7], due to their large surface area, integrated charge-transfer paths as well as morphological stability.[8]

As an important functional semiconductor with a direct wide band gap (3.37 eV) and a large exciton binding energy (60 meV), ZnO has attracted great interest owing to its potential applications in photocatalysis, solar cells, sensors, nanogenerators, room-temperature ultraviolet (UV) laser, optical waveguides, and so on.[9] Recently, $ZnGa_2O_4$, as a bimetallic semiconductor with spinel structure, have been investigated for technical application in photocatalytic fields.[10] Because its hybridized orbits of Ga4s4p and Zn4s4p, and the wider band gap (4.4 eV), $ZnGa_2O_4$ can promote the mobility of photogenerated electrons and improve the absorption efficiency in UV light radiation that would be the most available light source for waste water purification by photocatalytic degradation.[11] Generally, 1-D $ZnGa_2O_4$ could be synthesized by the chemical vapor deposition (CVD),[12] which requires a thin film ZnO template and multiple steps of high temperature process (>1000 ^oC). It is believed that complicated methods of material synthesis are not advantaged for further applications.[13] For this purpose, a facile synthesis method of 1-D $ZnGa_2O_4$ nanostructures is highly desirable for their scalable applications in photocatalytic fields.

It is well known that solution-liquid-solid (SLS) growth mechanism has been widely applied to prepare various continuous 1-D crystalline nanostructures via hydrothermal synthesis routes, in which low melting point metal (e.g., In, Ga and Sn, etc.) were used to induce the growth of 1-D nanostructures.[14] Previously, we have developed the SLS method under hydrothermal conditions for the growth of Sn-filled $In(OH)_3$ nanotubes[15] and twinned nanotowers and nanodendrites of HgSe[16]. Recently, we further develop Ga-mediated SLS growth strategy for the synthesis of novel Ga-doped, self-supported, independent aligned ZnO nanorods by one-pot hydrothermal synthesis.[17] Furthermore, topological-morphology-conversion (TMC) process has been proved to be one promising technique for the synthesis of newly nanostructured materials by means of chemical and structural transformation from established precursors with similar morphologies.[18] Most recently, we reported the synthesis of novel SnO_2-doped SiC hollow nanochains by TMC process from precursor of SnO_2@C core-shell nanochains.[19]

In this study, we demonstrate the controlled synthesis of $ZnGa_2O_4$ nanorod arrays from hexagonal ZnO microdishes, by using an efficient "SLS growth" and "TMC process" associated strategy. Firstly, the Ga-doped ZnO nanorod arrays were regularly synthesized by the Ga-mediated SLS hydrothermal synthesis[17], in which the hexagonal ZnO microdishes were transformed into aligned ZnO nanorods. Secondly, the $ZnGa_2O_4$ nanorod arrays were further synthesized by heat-treating TMC process from the Ga-doped ZnO nanorod arrays (see ESI for detailed synthetic steps). The newly designed 1-D semiconductor nanostructures of $ZnGa_2O_4$ nanorod arrays showed a very high activity for the photocatalytic degradation of Rhodamine B (RhB) under UV light radiation.

The phase structures of the as-synthesized samples have been characterized by XRD. Fig. 1 shows the XRD patterns of the hexagonal ZnO microdishes (black pattern), Ga-doped ZnO nanorod arrays (red pattern) and the $ZnGa_2O_4$ nanorod arrays (blue pattern). From the black and red patterns, it can be readily concluded that the two samples have the hexagonal phase structures of ZnO (JCPDS card No. 36-1451[9]). The sharp and clear diffraction peaks clearly indicate the good crystalline nature of the two products. It suggests the ideal ZnO structures have been obtained by the hydrolization of

$ZnSt_2$ under hydrothermal treatment. Expressly, from the red pattern no obvious Ga diffraction peak can be observed for Ga-doped ZnO sample, which is mainly due to the amorphous existence of Ga dopant as indicated by one of our previous work.[17] As illustrated by the blue pattern, the XRD pattern of the $ZnGa_2O_4$ sample can be indexed as cubic spinel $ZnGa_2O_4$ with a cell parameter of a=8.335 Å, agreeing well with the JCPDS Card No. 38-1240[10]. Several distinct peaks at 30.31, 35.71, 43.41, 57.41 and 63.01 match well with the (220), (311), (400), (511) and (440) crystal planes of $ZnGa_2O_4$, respectively. There is negligible ZnO component remained in the $ZnGa_2O_4$ sample. Therefore, the results indicate that $ZnGa_2O_4$ phase has been successfully synthesized from Ga-doped ZnO phase via the heat-treating conversion process.

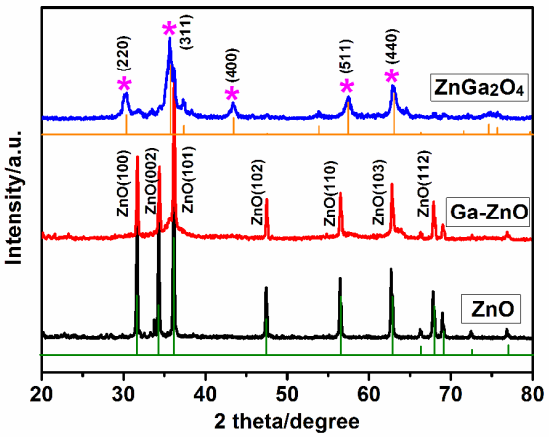

Fig 1. XRD pattern of hexagonal ZnO microdishes (black), Ga-ZnO nanorod arrays (red) and $ZnGa_2O_4$ nanorod arrays (blue).

At the same time, the schematic illustrations of crystal structures for $ZnGa_2O_4$ are illustrated in Fig. 2. The ball-and-stick model (Fig. 2 (a)) shows the typical cubic unit cell of spinel $ZnGa_2O_4$, corresponding to the XRD data. Fig. 2 (b) displays the crystallographic shear of $ZnGa_2O_4$, where zinc/oxygen tetrahedrons are showed in yellow parts. For one unit cell of $ZnGa_2O_4$, 32 O^{2-} constitute close-packed sub unit cell with face-centred-cubic structure, 8 Zn^{2+} occupy 8 tetrahedral vacancy (accounting for 1/8 of the total number of tetrahedral vacancy) to form 4 A-sites, and 16 Ga^{3+} occupy 16 octahedral vacancy (accounting for 1/2 of the total number of octahedral vacancy) to form 4 B-sites, where one complete unit cell of spinel $ZnGa_2O_4$ is made up of the 4 A-sites and 4 B-sites by alternate permutation.

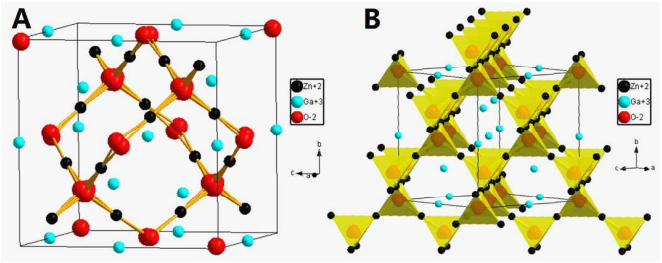

Fig 2. Schematic illustrations of crystal structures for $ZnGa_2O_4$: (a) A ball-and-stick model and (b) the crystallographic shear, zinc/oxygen tetrahedrons are showed in yellow parts.

To investigate the detailed nanostructures and morphological evolution of the as-prepared samples, FE-SEM and TEM characterization were further implemented. Fig. 3 shows the representative SEM images of the hexagonal ZnO microdishes. The lower-magnification images (Figs. 3 A and B) indicate that the sample has an interesting configuration comprising homologous 3-D hexagonal microdishes. The higher-magnification images (Figs. 3 C and D) reveal that the flowerpot is made up of one side hexagonal pot and the other side short nanorods (just like one flowerpot).

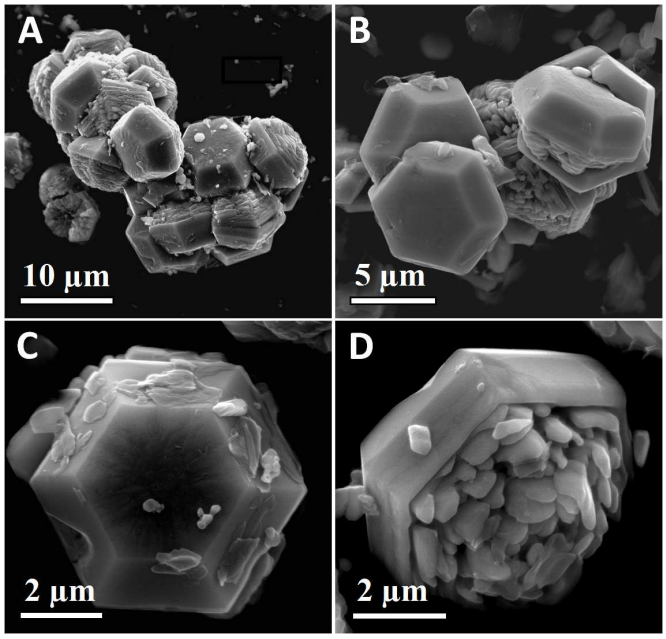

Fig 3. Representative SEM images of hexagonal ZnO microdishes.

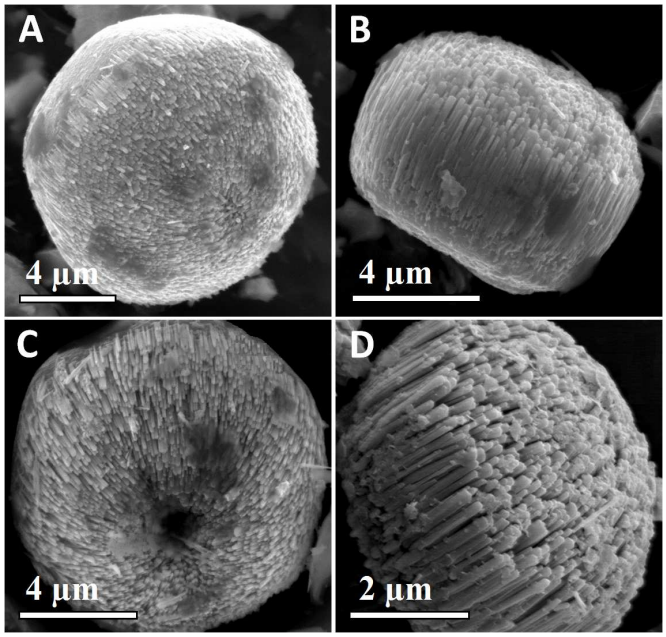

Fig 4. Representative SEM images of the nanorod arrays: (A, B) Ga-ZnO, (C, D) $ZnGa_2O_4$.

Figs. 4 A and B shows the representative SEM images of Ga-doped ZnO nanorod arrays. Evidently, the sample has highly self-supported aligned 1-D nanostructures, where the ZnO nanorods are vertically and well assembled into micro-architectures without the extraneous supporting substrates. These results demonstrate that ZnO 1-D nanostructures have been achieved by the Ga-mediated SLS hydrothermal process. Figs. 4 C and D shows the representative SEM images of $ZnGa_2O_4$ nanorod arrays, which reveals the loosely aligned 1-D nanostructures relative to the Ga-doped ZnO sample. Fig. 5 shows the SEM-EDS elemental mapping of Ga, Zn and O from the individual $ZnGa_2O_4$ nanorod array. It is found that the Ga,

Zn and O three elements (Figs. 5 B-D) are homogeneously distributed corresponding to the SEM image (Fig. 5 A).

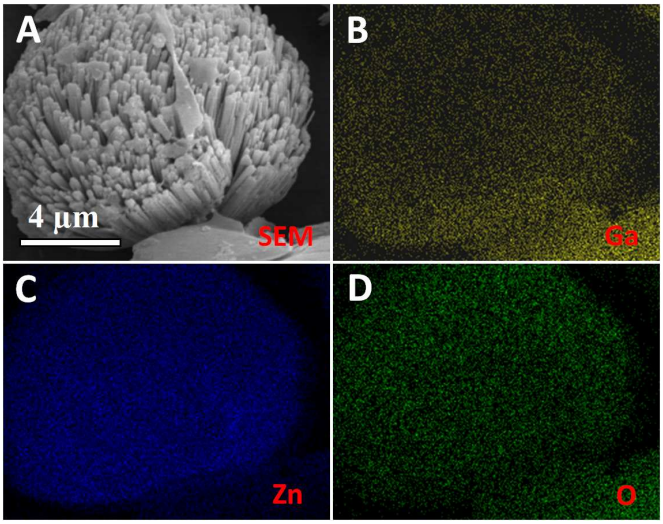

Fig 5. SEM-EDS elemental mapping images from the $ZnGa_2O_4$ nanorod array.

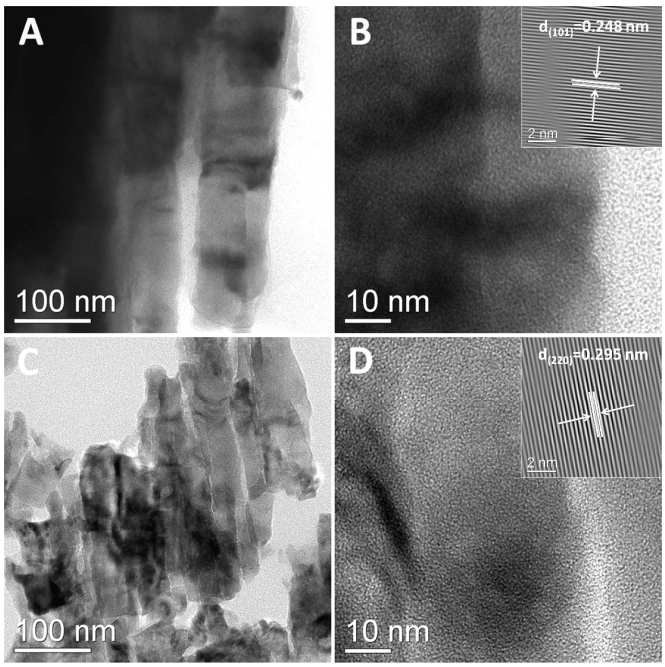

Fig 6. TEM images of the (A, B) Ga-ZnO nanorods and (C, D) $ZnGa_2O_4$ nanorods.

Fig. 6 shows the TEM images of Ga-doped ZnO nanorods (Figs. 6 A and B) and $ZnGa_2O_4$ nanorods (Figs. 6 C and D). It can be observed that the two samples have both dense aligned nanorod architectures with single nanorods of 50~80 nm diameter. A spot of nanopores existed in the $ZnGa_2O_4$ nanorods (see Fig. 6 D) might originate from the crystal defects during structure conversion process. The insets in Figs. 6 B and D further indicate the (101) planes of ZnO (d = 0.248 nm) and the (220) planes of $ZnGa_2O_4$ (d = 0.295 nm), respectively. The above-mentioned results largely demonstrate the feasibility of topological morphology conversion of Ga-doped ZnO nanorods to $ZnGa_2O_4$ nanorods by the heat-treating TMC process. In addition, the BET specific surface areas of $ZnGa_2O_4$ nanorods, Ga-doped ZnO nanorods and hexagonal ZnO microdishes were determined as 65.7, 61.2 and 38.4 $m^2 g^{-1}$, respectively.

The possible formation process of the $ZnGa_2O_4$ nanorod arrays, involving the evolvement of Ga-doped ZnO nanorods and $ZnGa_2O_4$ nanorods, are schematically shown in Fig. 7. In the absence of Ga during the hydrothermal process, the hexagonal ZnO microdishes were obtained (see Fig. 3 for details), indicating the Ga species plays an important role in the formation of ZnO 1-D framework.[17] Fig. 7 (i) illustrates a formation process of the Ga-doped ZnO nanorods with the SLS growth route. The SLS process maybe consist of four steps[14]: formation of the liquid Ga droplets in hydrothermal solution (S), production of ZnO by $ZnSt_2$ hydrolization and its diffusion to liquid Ga droplet to form liquid-solid (LS) interface, 1-D growth of the Ga-doped ZnO nanorods at the LS interface, and continuous 1-D growth of ZnO consumes the liquid Ga droplet, thus completing the SLS assembly of the Ga-doped ZnO nanorods. Fig. 7 (ii) illustrates the latent evolvement of the $ZnGa_2O_4$ nanorods from Ga-doped ZnO nanorods with the TMC process. In this process, the initial nanorods morphology of Ga-doped ZnO precursor would be inherited by $ZnGa_2O_4$ product by means of the potential chemical and structural transformation (ZnO react with Ga to form $ZnGa_2O_4$) under the heat-treating process. Further study on the accurate reaction mechanism is in progress.

Fig 7. Schematic illustration for the preparation of $ZnGa_2O_4$ nanorods: (i) Solution-Liquid-Solid (SLS) growth for Ga-doped ZnO nanorods and (ii) Topological-Morphology-Conversion (TMC) process for $ZnGa_2O_4$ nanorods.

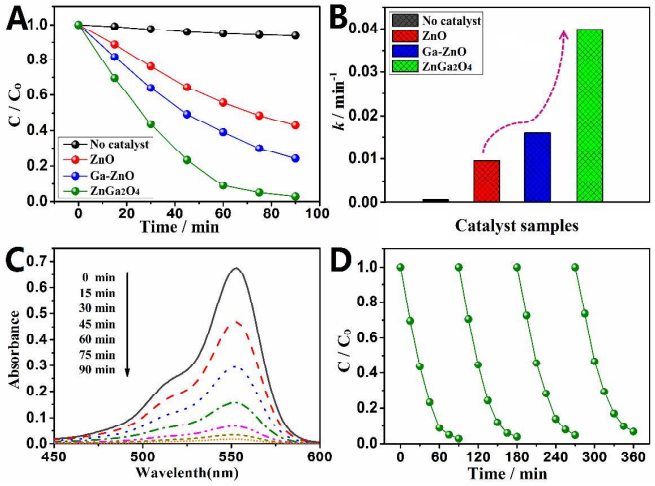

Fig 8. (a) Photocatalytic activities and (b) rate constant *k* of RhB degradation for the as-prepared photocatalysts; (c) absorption spectrum of RhB solution and (d) cycling runs for the degradation of RhB in the presence of $ZnGa_2O_4$ photocatalyst under UV light radiation.

The photocatalytic activities and stability of the as-prepared photocatalysts (the $ZnGa_2O_4$ nanorods, Ga-doped ZnO nanorods and hexagonal ZnO microdishes) were evaluated by degradation of RhB in aqueous solution under UV light radiation (see Fig. 8). Obviously, the $ZnGa_2O_4$ nanorods exhibit a much higher photocatalytic activity than the Ga-doped ZnO nanorods and hexagonal ZnO microdishes (Fig. 8 (a)), in which the RhB can be largely degraded (97.2%) in 90 min under UV light radiation, while the degradation rates of Ga-doped ZnO nanorods and hexagonal ZnO microdishes were only 75.9% and 57.1%, respectively. The first-order reaction rate constant can be calculated by the plots of the $\ln(C/C_0)$ v.s. radiation time (t). The obtained rate law may be $\ln(C/C_0) = -kt$, where C is the

concentration of dye, C_0 the initial concentration of dye, k the reaction rate constant, and t the irradiation time. The degradation rate constant k of $ZnGa_2O_4$ nanorods was estimated to be 0.0397 min^{-1}, which was 2.51 times and 4.22 times as high as those of Ga-doped ZnO nanorods (0.0158 min^{-1}) and hexagonal ZnO microdishes (0.0094 min^{-1}), respectively (Fig. 8 (b)). Fig. 8 (c) shows the change of absorption spectra of RhB solution when exposed to UV light at different times in presence of the photocatalyst of the $ZnGa_2O_4$ sample, which clearly shows that the absorption peak of RhB drops gradually with an increase of exposure time for 90 min (confirming the degradation of RhB as showed in Fig. 8 (a)). Furthermore, the stability testing of $ZnGa_2O_4$ sample illustrates that the degradation rate shows slightly decrease after four run repeated irradiation within 360 min (Fig. 8 (d)). The above mentioned results demonstrate that the obtained $ZnGa_2O_4$ nanorods can be used as a promising photocatalyst with excellent activity and desirable stability, for the degradation of RhB in aqueous solution under UV light radiation.

Actually, the physical dimensions and chemical compositions of semiconductors have significant effects on their physicochemical properties.[1] The smaller dimension of semiconductors often leads to the higher photocatalytic activity because their higher specific surface area along with optimized utilization efficiency.[2] Obviously, the specific surface area of Ga-doped ZnO nanorods (61.2 $m^2 g^{-1}$) is much higher than that of hexagonal ZnO microdishes (38.4 $m^2 g^{-1}$). Hence, the improved activity of Ga-doped ZnO nanorods relative to hexagonal ZnO microdishes can be attributed to the high surface area of nanorod structures. However, the specific surface areas of $ZnGa_2O_4$ nanorods (65.7 $m^2 g^{-1}$) and Ga-doped ZnO nanorods (61.2 $m^2 g^{-1}$) are more approximated, so the high activity of the $ZnGa_2O_4$ nanorods sample is largely due to its favorable material structures.

It is generally accepted that the superior photocatalytic activity of $ZnGa_2O_4$ originates in its unique electronic and band structures. For one thing, the bottom of conduction band (LUMO) is formed by Ga4s4p-Zn4s4p hybridized atomic orbits, which is able to promote the mobility of photogenerated electrons and beneficial to charge separation.[20] For another, the wider band gap (4.4 eV) endows the photogenerated charge with stronger reductive capability, which results in stronger redox ability of photogenerated electron-hole pairs, thus facilitating the photocatalytic activity.[21] In addition, the possible existence of trace heterojunction of ZnO-$ZnGa_2O_4$ may contribute to photocatalytic activity by the improved charge transfer. The accurate results are expected by further advanced characterization techniques.

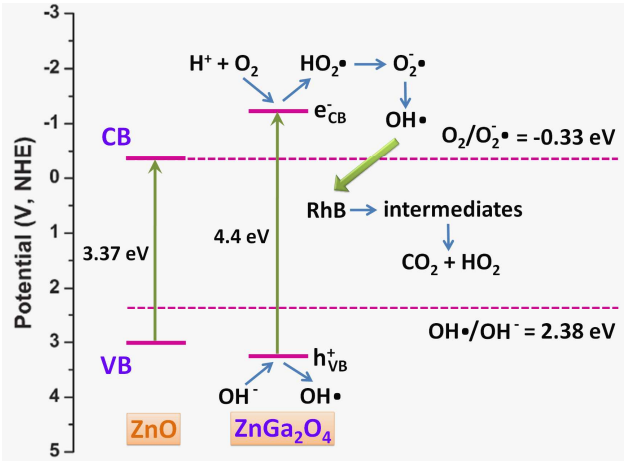

Fig 9. Schematic illustration for the band structures of ZnO and $ZnGa_2O_4$ and proposed pathway of RhB photocatalytic degradation.

For the sake of analysis of catalytic mechanism, the band structures of ZnO and $ZnGa_2O_4$ and possible pathway of RhB photocatalytic degradation are schematically illustrated in Fig. 9. In the case of $ZnGa_2O_4$, the E_{VB} is 3.15 V that is much higher than the 2.38 V of E(HO•/OH^-), and the E_{CB} is -1.25 V that is much lower than the -0.33 V of $E(O_2/O_2^-•)$.[11] In the case of ZnO, only the E_{CB} is lower than that of $E(O_2/O_2^-•)$. As a result, HO• can be more readily generated for $ZnGa_2O_4$ under UV light in RhB aqueous solution, leading the fact that $ZnGa_2O_4$ photocatalysts exhibited much higher photocatalytic properties than that of ZnO. The possible reaction process are as follows: once $ZnGa_2O_4$ catalyst generates the electron-hole pairs by UV light radiation, the photogenerated electrons (e^-) on conduction band (CB) will bond with adsorbed oxygen and water to form strong oxidizing species of O_2^-• and HO•, while the holes (h^+) on the valence band (VB) will also bond with adsorbed oxygen and water to form HO•. Under the action of substantial strong oxidizing species, the structure of RhB was destroyed and finally decomposed into CO_2 and H_2O. All these processes might be described as follows.[22]

$$e^- + O_2 \rightarrow •O_2^- \quad (1)$$

$$•O_2^- + e^- + 2H^+ \rightarrow H_2O_2 \quad (2)$$

$$H_2O_2 + e^- \rightarrow •OH + OH^- \quad (3)$$

$$h^+ + H_2O \rightarrow •OH + H^+ \quad (4)$$

$$•OH + RhB \rightarrow CO_2 + H_2O \quad (5)$$

It is well known that plenty of materials have been available for photocatalytic degradation of RhB, including the TiO_2[23], ZnO[24], AgBr[25], Ag_3PO_4[26], BiOBr[27], $BiPO_4$[28] as well as $ZnGa_2O_4$. The TiO_2 is the most extensively studied and stable catalyst for photocatalytic degradation in scientific perspective. However, it is difficult to discuss whether of them is the most promising photocatalyst in real-time application, due to their different catalytic mechanism and cost of materials. In the present study, we report the controlled synthesis of self-supported $ZnGa_2O_4$ nanorod arrays by using an efficient "SLS growth" and "TMC process" associated strategy. Although it is difficult to discuss the superiority of $ZnGa_2O_4$ relative to TiO_2 on degradation of RhB, the proposed "SLS growth" and "TMC process" synthetic strategies may be of general significance in the preparation TiO_2 and other types of photocatalysts.

In conclusion, we demonstrated the controlled synthesis of $ZnGa_2O_4$ nanorod arrays from hexagonal ZnO microdishes for advanced application of photodegradation water purification. The as-prepared $ZnGa_2O_4$ sample has highly self-supported aligned 1-D nanostructures, where $ZnGa_2O_4$ nanorods with 50~80 nm diameter are vertically assembled into micro-architectures without the extraneous supporting substrates. The $ZnGa_2O_4$ nanorod arrays showed much higher BET specific surface areas over the hexagonal ZnO microdishes. Due to favorable 1-D nanostructures and unique electronic band structures, the $ZnGa_2O_4$ photocatalyst exhibited a much higher photocatalytic activity relative to the hexagonal ZnO microdishes, in which the degradation rate of RhB can be 4.22 times as high as that of ZnO photocatalyst. The findings suggest that this new-fashioned architecture of $ZnGa_2O_4$ could be used as a promising photocatalytic material for organic dye degradation.

Acknowledgements

This research was supported by the National Natural Science Foundation of China (21173088 and 21105030), Natural Science Foundation of Guangdong Province (S2013040015162), Guangdong Province and Chinese Academy of Sciences Strategic Cooperative Project (2012B090400003), Science and Technology Project of Maoming (2014006) and Doctor Startup Project of school (513086).

Notes and references

1 A. Alivisatos, *J. Phys. Chem.*, 1996, **100**, 13226-13239.
2 Z. Zhuang, Q. Peng and Y. Li, *Chem. Soc. Rev.*, 2011, **40**, 5492-5513.
3 T. Zhai, L. Li, Y. Ma, M. Liao, X. Wang, X. Fang, J. Yao, Y. Bando and D. Golberg, *Chem. Soc. Rev.*, 2011, **40**, 2986-3004.
4 A. Hochbaum and P. Yang, *Chem. Rev.*, 2010, **110**, 527-546.
5 (a) T. Wang, Z. Jiao, T. Chen, Y. Li, W. Ren, S. Lin, G. Lu, J. Ye and Y. Bi, *Nanoscale*, 2013, **5**, 7552-7557; (b) M. Lv, D. Zheng, M. Ye, J. Xiao, W. Guo, Y. Lai, L. Sun, C. Lin and J. Zuo, *Energ. Environ. Sci.*, 2013, **6**, 1615-1622.
6 (a) L. Pan, H. Huang, C. Lim, Q. Hong, M. Tse and O. Tan, *RSC Adv.*, 2013, **3**, 3566-3571; (b) M. Sun, X. Ma, X. Chen, Y. Sun, X. Cui, Y. Lin, *RSC Adv.*, 2014, **4**, 1120-1127.
7 M. Nischk, P. Mazierski, M. Gazda and A. Zaleska, *Appl. Catal. B-Environ.*, 2014 **144**, 674-685.
8 C. Zhang, H. Yu, Y. Li, L. Fu, Y. Gao, W. Song, Z. Shao, B. Yi, *Nanoscale*, 2013, **5**, 6834-6841.
9 (a) S. Xu and Z. Wang, *Nano Res.*, 2011, **4**, 1013-1098; (b) C. Lai, X. Wang, Y. Zhao, H. Fong and Z. Zhu, *RSC Adv.*, 2013, **3**, 6640-6645.
10 (a) L. Liu, J. Huang, L. Cao, J. Wu, J. Fei, H. Ouyang, F. Ma and C. Zhou, *Mater. Lett.*, 2013, **95**, 160-163; (b) S. Yan, S. Ouyang, J. Gao, M. Yang, J. Feng, X. Fan, L. Wan, Z. Li, J. Ye, Y. Zhou and Z. Zou, *Angew. Chem.*, 2010, **122**, 6544-6548.
11 (a) W. Zhang, J. Zhang, Z. Chen and T. Wang, *Catal. Commun.*, 2009, **101**, 781-1785; (b) W. Zhang, J. Zhang, X. Lan, Z. Chen and T. Wang, *Catal. Commun.*, 2010, **11**, 1104-1108.
12 M. Zhong, Y. Li, T. Tokizono, M. Zheng, I. Yamada and J Delaunay, *J Nanopart. Res.*, 2012, **14**, 804-814.
13 L. Tien, C. Tseng, Y. Chen and C. Ho, *J. Alloy. Compound.*, 2013, **555**, 325-329.
14 (a) H. Yu and W. Buhro, *Adv. Mater.*, 2003, *15*, 416-419; (b) J. Sun, L. Wang, and W. Buhro, *J. Am. Chem. Soc.*, 2008, **130**, 7997-8005.
15 Y. Fang, X. Wen and S. Yang, *Angew. Chem.*, 2006, **118**, 4771-4774.
16 A. Qin, X. Zhou, Y. Qiu, Y. Fang, C. Su and S. Yang, *Adv. Mater.*, 2008, **207**, 68-773.
17 S. Yang, C. Ge, Z. Liu, Y. Fang, Z. Li, D. Kuang and C. Su, *RSC Adv.*, 2011, **1** 1691-1694.
18 (a) L. Tian, H. Zou, J. Fu, X. Yang, Y. Wang, H. Guo, X. Fu, C. Liang, M. Wu, P. Shen and Q. Gao, *Adv. Funct. Mater.*, 2010, **20**, 617-623; (b) J. Kim, B. Fang, M. Song and J. Yu, *Chem. Mater.*, 2012, **24**, 2256-2264.
19 X. Zhou, Y. Liu, X. Li, Q. Gao, X. Liu and Y. Fang, *Chem. Commun.*, 2014, **50**, 1070-1073.
20 S. Sampath, D. Kanhere and R. Pandey, *J. Phys-Condens. Mat.*, 1999, **11**, 3635.
21 S. Bae, J. Lee, H. Jung, J. Park and J. Ahn, *J. Am. Chem. Soc.*, 2005, **127**, 10802-10803.
22 G. Chen, M. Sun, Q. Wei, Y. Zhang, B. Zhu and B. Dua, *Chem. Soc. Rev.*, 2012, **41**, 782-796.
23 J. Zhang, Z. Zhu, Y. Tang, X. Feng, *J. Mater. Chem. A*, 2013, **1**, 3752-3756.
24 B. Weng, M. Yang, N. Zhang, Y. Xu, *J. Mater. Chem. A*, 2014, **2**, 9380-9389.
25 J. Wang, C. An, J. Liu, G. Xi, W. Jiang, S. Wang, Q. Zhang, *J. Mater. Chem. A*, 2013, **1**, 2827-2832.
26 H. Li, S. Yin, Y. Wang, T. Sekino, S.W. Lee, T. Satoa, *J. Mater. Chem. A*, 2013, **1**, 1123-1126.
27 D. Zhang, J. Li, Q. Wang, Q. Wu, *J. Mater. Chem. A*, 2013, **1**, 8622-8629.
28 C. Pan, J. Xu, Y. Chen, Y. Zhu, *Appl. Catal. B-Environ.*, 2012, **115-116**, 314-319.